NASA/TP–20260001601

Fatigue Life of Flow-Formed Aluminum 2195 and 6061 Alloys

Andrew Boddorff, John Newman, Wesley Tayon
Langley Research Center, Hampton, Virginia

Elizabeth Urig

Analytical Mechanics Associates, Hampton, Virginia

March 2026

NASA STI Program Report Series

Since its founding, NASA has been dedicated to the advancement of aeronautics and space science. The NASA scientific and technical information (STI) program plays a key part in helping NASA maintain this important role.

The NASA STI program operates under the auspices of the Agency Chief Information Officer. It collects, organizes, provides for archiving, and disseminates NASA's STI. The NASA STI program provides access to the NTRS Registered and its public interface, the NASA Technical Reports Server, thus providing one of the largest collections of aeronautical and space science STI in the world. Results are published in both non-NASA channels and by NASA in the NASA STI Report Series, which includes the following report types:

- TECHNICAL PUBLICATION. Reports of completed research or a major significant phase of research that present the results of NASA Programs and include extensive data or theoretical analysis. Includes compilations of significant scientific and technical data and information deemed to be of continuing reference value. NASA counterpart of peer-reviewed formal professional papers but has less stringent limitations on manuscript length and extent of graphic presentations.

- TECHNICAL MEMORANDUM. Scientific and technical findings that are preliminary or of specialized interest, e.g., quick release reports, working papers, and bibliographies that contain minimal annotation. Does not contain extensive analysis.

- CONTRACTOR REPORT. Scientific and technical findings by NASA-sponsored contractors and grantees.

- CONFERENCE PUBLICATION. Collected papers from scientific and technical conferences, symposia, seminars, or other meetings sponsored or co-sponsored by NASA.

- SPECIAL PUBLICATION. Scientific, technical, or historical information from NASA programs, projects, and missions, often concerned with subjects having substantial public interest.

- TECHNICAL TRANSLATION. English-language translations of foreign scientific and technical material pertinent to NASA's mission.

Specialized services also include organizing and publishing research results, distributing specialized research announcements and feeds, providing information desk and personal search support, and enabling data exchange services.

For more information about the NASA STI program, see the following:

- Access the NASA STI program home page at http://www.sti.nasa.gov

- Help desk contact information:

https://www.sti.nasa.gov/sti-contact-form/
and select the "General" help request type.

NASA/TP–20260001601

Fatigue Life of Flow-Formed Aluminum 2195 and 6061 Alloys

Andrew Boddorff, John Newman, Wesley Tayon, and Elizabeth Urig
Langley Research Center, Hampton, Virginia

Elizabeth Urig

Analytical Mechanics Associates, Hampton, Virginia

National Aeronautics and
Space Administration

Langley Research Center
Hampton, Virginia 23681-2199

March 2026

Acknowledgments

The authors wish to express gratitude to Harold "Clay" Claytor for his help preparing samples for testing and characterization. Additionally, the authors wish to express gratitude to the Green Aviation and Transformational Tools and Technologies programs for the funding, especially Dr. Edward Glaessgen for his support.

Available from:

NASA STI Program / Mail Stop 050
NASA Langley Research Center
Hampton, VA 23681-2199

Table of Contents

1.0 Introduction **1**
2.0 Experimental **2**
2.1 Materials 2
2.2 Residual Stress Measurement 3
2.3 Fatigue Life Testing 4
2.4 Fractography 6
3.0 Results and Discussion **6**
3.1 Residual Stress 6
3.2 Fatigue Life 8
3.3 Fractography 11
4.0 Conclusion **16**
5.0 References **18**
Appendix A. Full Organizational Model **21**

List of Figures

Figure 1. Pictures of the a) 8-inch Al-Li 2195 integrally stiffened cylinder and b) 120-inch aluminum 6061 integrally stiffened cylinder. 3
Figure 2. Full heat-treated sample (a) geometry as measured with the structured light scanner, before wire EDM extraction of (b), the location of which is shown in (a) as dotted lines. After the characterization of distortion of (b), the sample undergoes a secondary wire EDM operation, yielding samples (c) and (d). 4
Figure 3. Drawing of the fatigue life specimen with dimensions in inches. 5
Figure 4. The specimen orientations relative to original material is shown for a) the flow-formed Al-Li 2195 specimen extracted from the wall of the cylinder (red outline), b) top-down view of the wrought Al-Li 2195 specimens extracted in the rolling direction (black outline) and at the 45º angle between L and LT direction (green outline), c) side on view of the specimen extraction of wrought Al-Li 2195 (blue rectangles), and d) top-down view of flow-formed Al 6061 specimens extracted from the wall in the axial direction (parallel to the integral stiffeners [white outline]) and in the circumferential direction (perpendicular to integral stiffeners [orange outline]). 6
Figure 5. Circumferential deflections (a-b), and axial deflection (c) after averaging and smoothing, showing the distributions in the stiffener (a), thin wall (b), and axial direction (c) of flow-formed Al-Li 2195 cylinder. 7
Figure 6. von Mises stress distributions in the circumferential direction of the flow-formed Al-Li 2195 cylinder, comparing the distributions and magnitudes between the stiffener (left) and thin wall (right). 8
Figure 7. von Mises stress distributions in the axial direction of the Al-Li 2195 cylinder. The boxed and expanded region is the stiffener. 8
Figure 8. The S-N curve for the flow-formed Al 6061 (blue) compared to wrought material (black) taken from literature [17]. 9
Figure 9. The S-N curves for the flow-formed (blue) and wrought (black) Al-Li 2195. 10
Figure 10. The S-N curves for the flow-formed Al-Li 2195 tested at room temperature (black) and at cryogenic temperature (-321ºF; -196ºC; blue). 11

Figure 11. Representative fatigue test specimen fracture surfaces from flow-formed a) Al 6061, b) flow-formed Al-Li 2195, c) wrought Al-Li 2195 and d) flow-formed Al-Li Al 2195 tested at cryogenic temperatures. (Left) Optical image and (right) profilometry image both generated from Keyence microscope. Dashed black line denotes the fatigue crack front. 12
Figure 12. EBSD inverse pole figure map indicating recrystallization within the wall of the Al-Li 2195 flow-formed cylinder. 15
Figure 13. EBSD pole figures from a) Al-Li 2195 flow-formed wall section (RD = axial direction and TD = radial direction of the flow-formed cylinder) and b) rolled Al-Li 2195 plate. 16

List of Tables

Table 1. List of the fatigue life specimens tested. 5
Table 2. Results from fatigue life testing from all specimens tested. 21

Nomenclature

Al	Aluminum
EBSD	Electron backscattered diffraction
EDM	Electrical Discharge Machining
FEM	Finite Element Model
GPa	Gigapascal
ksi	Kilopounds per square inch
L-LT	Longitudinal-long-transverse
Li	Lithium
LT	Long-transverse
MPa	Megapascal
MSI	Million pounds per square inch
MVC	Microvoid coalescence
OML	Outer mold line
S-T	Short-transverse
SHT	Solution heat treatment
μin	Microinch
μm	Microns or micrometer
δ’	Delta prime phase

Abstract

The successful design and fabrication of metallic cryotanks for commercial aviation applications require lightweight, durable materials capable of withstanding high pressures and cryogenic temperatures through tens of thousands of thermomechanical refueling cycles. Flow forming is an advanced manufacturing technique that offers high-rate production and scalability for fabricating integrally stiffened cylinders suitable for cryotank applications. This work establishes the durability of flow-formed aluminum alloys by characterizing their fatigue life performance under conditions that mimic cryotank refueling cycles. Residual stresses in flow-formed aluminum-lithium (Al-Li) 2195-T6 cylinders were assessed using the contour method and found to be minimal. Fatigue life testing was conducted on flow-formed Al-Li 2195-T6 at room temperature and cryogenic temperatures (-321°F [-196°C]), with wrought Al-Li 2195-T6 serving as a baseline for comparison. Results showed that flow-formed materials exhibited fatigue performance comparable to or better than wrought materials, with no statistically significant differences observed between different specimen orientations relative to processing directions. Fractography revealed reduced delaminations in the flow-formed Al-Li 2195 samples as compared to wrought, indicating potential improvement to the microstructure that could result in improved service properties. Texture analysis using electron backscattered diffraction (EBSD) indicated recrystallization during heat treatment, potentially contributing to reduced delamination susceptibility. These findings demonstrating flow-formed material durability coupled with the high manufacturing efficiency of flow forming, makes flow forming an attractive process to produce aircraft cryotanks.

1.0 Introduction

The design and fabrication of cryotanks suitable for commercial aviation present numerous unique challenges in containing fuels at high-pressures (4350 psi [300 bar]) or at low temperatures (as low as -423ºF [-253ºC]) while delivering a lightweight, reliable solution [1–4]. Aluminum cryotanks, specifically the aluminum-lithium alloy 2195 (Al-Li 2195), have been used in space flight (e.g., SpaceX's Falcon 9) or developmental hydrogen-powered cars [5], however both applications have different requirements than aviation. Cryotanks for space flight, even the reusable versions, do not need to sustain tens of thousands of thermomechanical refueling cycles that are required in aviation. For liquid hydrogen powered automotives, alternatives to petroleum are being sought due to energy security and carbon emissions [6]. Automotive cryotanks have more similar refueling behavior to commercial aviation, though do not need to focus on a lightweight design [2]. At the present, the durability demands of cryotanks for aviation point towards a metallic design, as the composite alternatives have not demonstrated the required level of durability [1].

The replacement of jet-fuel-powered aircraft with cryogenic fuels requires scalable and high-rate manufacturing approaches for tank fabrication to meet the growing demands from the aerospace industry. Flow forming is an advanced manufacturing technique that is capable of meeting the requirements of high manufacturing rates and scalability [7,8]. Flow forming is an incremental forming technique that involves rotating a preform and using rollers to plastically deform the material against a mandrel. The resulting flow-formed part geometry has reduced wall thickness and increased length. The flow forming process is capable of producing integrally stiffened cylinders and shapes conducive to cryotank fabrication [9,10]. Flow forming appears to be well-suited to the task of fabricating cryotanks, however the material properties, specifically durability, of the formed parts need to be established.

The materials used in the aircraft cryotanks must have a high specific strength, stiffness, durability, crashworthiness, toughness, and low susceptibility to hydrogen embrittlement. Flow-formed aluminum specimens have demonstrated equivalent, if not better, yield strength, ultimate strength, toughness, and ductility [10,11]. The flow forming process induces a high-level of strain into the material, but the durability of flow-formed materials has not been explored. Additionally, the material performance at cryogenic temperatures remains to be demonstrated. The initial studies of flow-forming properties shows promise for use in cryogenic tanks; however, the issue of durability still remains unaddressed [9–11].

This work aims to establish the durability of flow-formed aluminum alloys by mimicking the mechanical cycling of cryotanks during refueling. First, characterization and assessment of the impact of residual stresses on fatigue life is performed. Second, the fatigue life of flow-formed and wrought Al-Li 2195 and Al 6061 at room temperature and at cryogenic temperatures (-321ºF [-196ºC]) is determined at various sample orientation relative to processing directions. Wrought Al-Li 2195 is the conventional product form for Al-Li 2195, thus is used as a baseline. Third, fractography of the failed wrought and flow-formed specimens is compared and discussed. Finally, the viability of flow-forming as a future manufacturing process for production of aircraft cryotanks is provided in the conclusion.

2.0 Experimental

2.1 Materials

The flow-formed, integrally stiffened Al-Li 2195 cylinder and Al 6061 cylinders from which specimens were cut are shown in Figure 1a and b, respectively. The Al-Li 2195 cylinder is 8 inches in diameter and was manufactured in 2013 [12]. The wrought Al-Li 2195 specimens were taken from an unused flow-forming blank from the 2013 forming effort [12]. The Al 6061 cylinder is 120 inches in diameter and was manufactured in 2019 [9]. Descriptions of the development and manufacturing process of these cylinders are provided by Tayon et al. [9]. The flow-formed and wrought Al-Li 2195 materials were solution heat treated at 950ºF (510ºC) in a salt bath, water quenched, and aged at 302ºF (150ºC) for 25 hours to T6 following AMS2770R. The flow-formed Al 6061 cylinder was previously heat treated to the T6 condition [9]. In this report, any references to Al-Li 2195 and Al 6061 are assumed to be in the T6 condition.

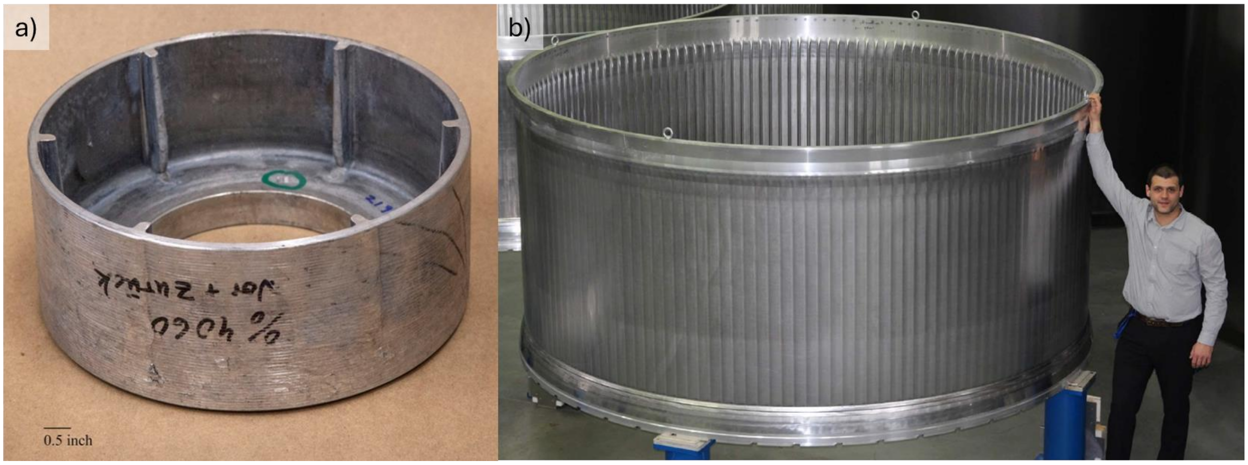

Figure 1. Pictures of the a) 8-inch Al-Li 2195 integrally stiffened cylinder and b) 120-inch Al 6061 integrally stiffened cylinder.

2.2 Residual Stress Measurement

To estimate the residual stress held within the heat-treated Al-Li flow-formed cylinder, the contour method of estimation was used. The contour method destructively characterizes the residual stress by making a precision cut and measuring the resultant deflections on either side of the cut. The measured deflections are inputted into a Finite Element Model (FEM) as elastic displacement, which quantifies the residual stress distribution required to generate the measured deflections. Prime and DeWald detail the origins and best practices associated with contour method, which include utilizing the law of superposition to determine residual stress on multiple surfaces, and assuming machining distortion is negligible [13–15].

The original geometry was nondestructively captured after heat treatment using a Creaform Metrascan 750 Elite structured light scanner, which is capable of measuring 3D objects with a resolution up to 100 µm. The original scanned geometry was used as the input geometry for the finite element model and is shown in Figure 2a. The cylinder was cut with wire Electrical Discharge Machining (EDM) to minimize machining distortion effects on the resultant deflection. Figure 2 shows the location of the wire EDM cuts. Cut locations were selected to determine residual stress axially and radially through the thin wall region and within the stiffener.

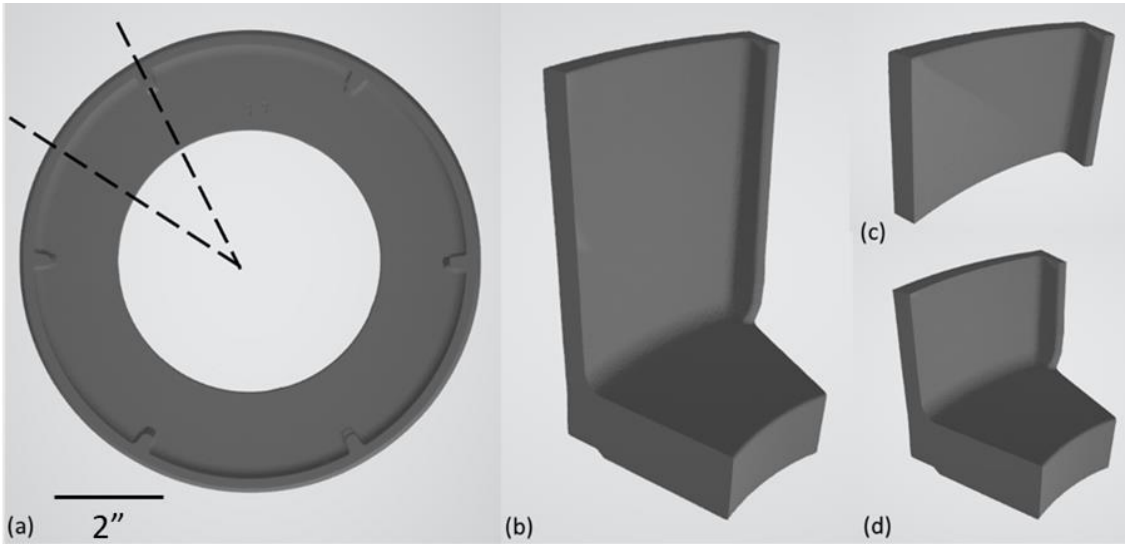

Figure 2. Full heat-treated sample (a) geometry as measured with the structured light scanner, before wire EDM extraction of (b), the location of which is shown in (a) as dotted lines. After the characterization of distortion of (b), the sample undergoes a secondary wire EDM operation, yielding samples (c) and (d).

The sample was cut along the dashed lines indicated in Figure 2a, which resulted in the sample shown in Figure 2b. The Figure 2b sample deflection was measured as an intermediate step using a profilometer before being cut axially, fabricating Figure 2c and Figure 2d samples. The cut geometry faces were measured using a Keyence VR-6000 optical profilometer, which can collect topographic data to a resolution of 4 µin (0.1 µm). The collected displacement data was averaged and denoised in preparation for use as a displacement field in the finite element model.

The FEMs were run in Altair Hyperworks™ with nodal displacement applied to the cut surfaces. The material model was based on Al-Li 2195 elastic properties, with a Young’s modulus of 10 MSI (69 GPa) and a Poisson’s ratio of 0.3 [16]. The models were constructed using the light scanned geometry as the outer shell. The full section shown in Figure 2b was meshed with 46,000 tetrahedral elements, which corresponded to an average element edge length of 0.08 in (2 mm). The axial secondary models in Figure 2c and Figure 2d maintained the average edge length of 0.08 in (2 mm), which corresponded to approximately 23,000 tetrahedral elements.

2.3 Fatigue Life Testing

The fatigue specimens were extracted via wire EDM, and the specimen design is shown in Figure 3. The entire specimen was polished to 1200 grit to avoid any cracking from surface flaws during fatigue life testing. The list of specimens extracted at each orientation is provided in Table 1. The orientation of each specimen relative to the parent material is shown in Figure 4. A servo-hydraulic test machine was used to perform fatigue life testing according to ASTM E466 with an R-ratio of 0.1, at a range of mean stresses, and at 5Hz frequency on specimens shown in Table 1. Ten flow-formed Al-Li 2195 samples were fatigue life tested at -321ºF (-196ºC) at Westmoreland Mechanical Testing and Research using the same R-ratio and frequency as other samples with a run out of 2 million cycles (5 million for one sample).

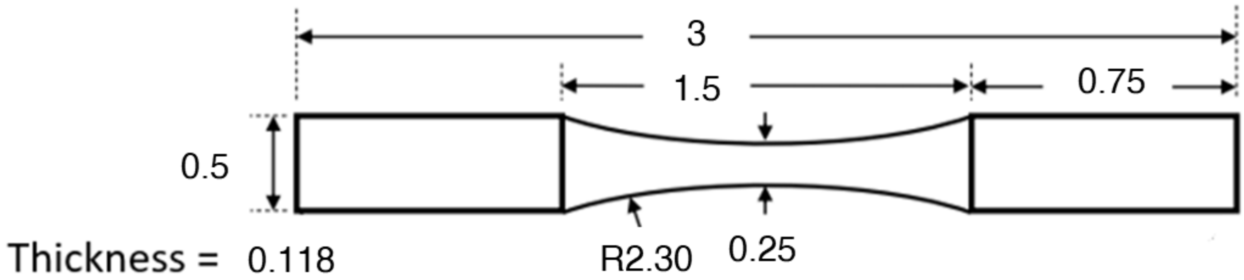

Figure 3. Drawing of the fatigue life specimen with dimensions in inches.

Table 1. List of the fatigue life specimens tested.

Alloy	Manufacturing Method	Orientation	Temperature (°F)	Mean Stress Range (ksi)	Number of Specimens
Al-Li 2195-T6	Flow-forming	Parallel to stiffeners (Figure 4a, red)	70 (21°C)	39-59 (269 – 407 MPa)	15
			-321 (-196°C)	37-60 (255 – 414 MPa)	10
	Wrought	Rolling Direction (L) (Figure 4b, black)	70 (21°C)	34-57 (234 – 393 MPa)	10
		45° (Figure 4b, green)			10
Al 6061-T6	Flow-forming	Parallel to stiffeners (Figure 4b, white)	70 (21°C)	29-52 (200 – 359 MPa)	10
		Perpendicular to stiffeners (Figure 4b, orange)			10

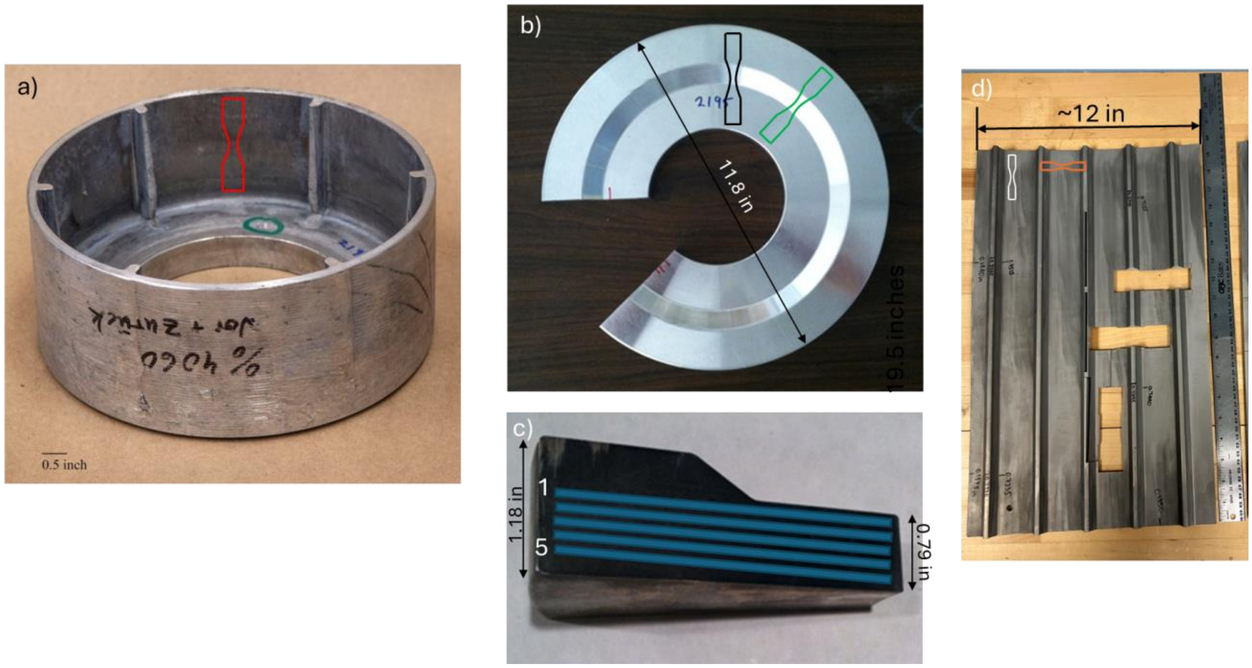

Figure 4. The specimen orientations relative to original material is shown for a) the flow-formed Al-Li 2195 specimen extracted from the wall of the cylinder (red outline), b) top-down view of the wrought Al-Li 2195 specimens extracted in the rolling direction (black outline) and at the 45º angle between L and LT direction (green outline), c) side on view of the specimen extraction of wrought Al-Li 2195 (blue rectangles), and d) top-down view of flow-formed Al 6061 specimens extracted from the wall in the axial direction (parallel to the integral stiffeners [white outline]) and in the circumferential direction (perpendicular to integral stiffeners [orange outline]).

2.4 Fractography

Fractography was performed on failed fatigue test specimens to correlate crack morphology with test results and identify any potential anomalies within the test that may be tied with underlying microstructure or flaws. Optical microscopy and profilometry images were collected using a Keyence VR-6000 microscope to characterize the fracture surfaces. The optical images provided visual documentation of the fracture surface features. Profilometry maps were computed based on changes in light reflectivity from the surface features, enabling measurement of topographical data of the fracture surface such as depth, roughness, angle, etc.

3.0 Results and Discussion

3.1 Residual Stress

The resultant circumferential and axial deflection fields for flow-formed Al-Li 2195 are shown in Figure 5a-b and Figure 5c, respectively. Note that color scale bars are different for each contour plot in Figure 5. Based on the contour plots in Figure 5, the magnitude of deflections was small. The total range of deflection circumferentially through the stiffener was 2420 μin (61.5 μm) and through the thin wall was 3980 μin (101 μm). While these measurements are within the measurable tolerance of the profilometer (resolution 4 μin [0.1 μm]), the values indicate minimal spring back and deflection. The distributions of the deflections indicate that the middle of the thick baseplate provided enough rigidity to prevent distortion, while the thin wall and stiffener deflected more broadly.

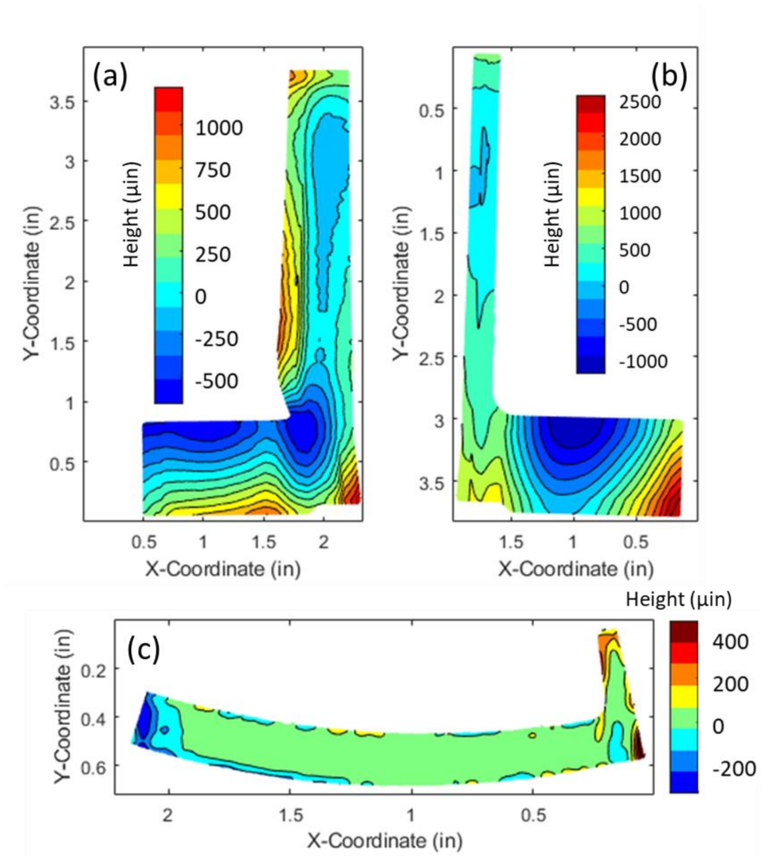

Figure 5. Circumferential deflections (a-b), and axial deflection (c) after averaging and smoothing, showing the distributions in the stiffener (a), thin wall (b), and axial direction (c) of flow-formed Al-Li 2195 cylinder.

The averaged contour plot in Figure 5c for the axial deflection measurements showed even less distortion than the circumferential measurements. The total range of deflection was 861 µin (21.9 µm). It is assumed that most internal stresses were relieved through the primary cut and minimal stress relief occurred during the secondary machining operation.

Figure 6 and 7 show the resultant von Mises stress distributions generated from the FEM for the circumferential and axial directions. Figure 6 shows both the thin wall and stiffener have minor residual stress with a maximum residual stress of 2.2 ksi (15.1 MPa) occurring in the thick clamp region. However, the through stiffener region shows a consistent stress averaging 0.9 ksi (6 MPa) compared to 0.19 ksi (1.3 MPa) in the thin wall, indicating the stiffener formation generated more residual stress over the thin wall forming. Moreover, inspection of von Mises stress distributions in the axial direction (Figure 7) shows the same trend, where the stiffener is observed to carry approximately 2 ksi (13.7 MPa) of stress compared to nominally zero stress through the thin wall.

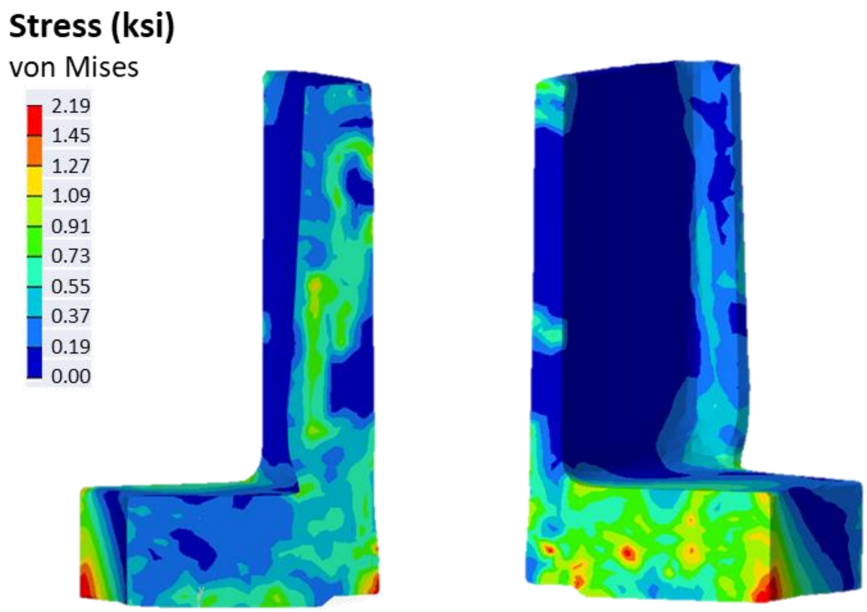

Figure 6. von Mises stress distributions in the circumferential direction of the flow-formed Al-Li 2195 cylinder, comparing the distributions and magnitudes between the stiffener (left) and thin wall (right).

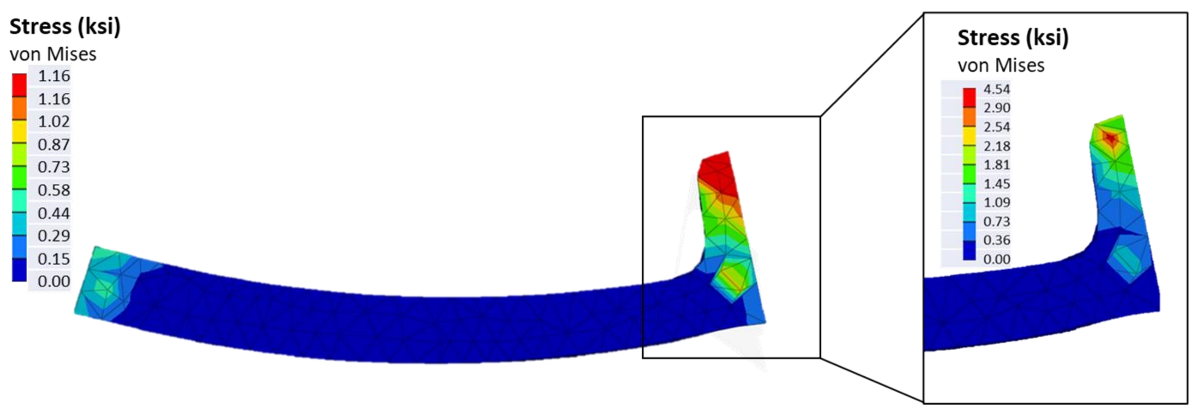

Figure 7. von Mises stress distributions in the axial direction of the Al-Li 2195 cylinder. The boxed and expanded region is the stiffener.

Based on the low estimated residual stresses seen in the bulk of the flow-formed cylinder, it can be assumed that the T6 heat treatment was sufficient to remove any residual stresses that may have been generated in the as-formed cylinder, and residual stress effects can be treated as negligible for fatigue life testing.

3.2 Fatigue Life

The S-N curves generated from the fatigue life experiments on flow-formed and wrought Al-Li 2195 are rationalized based on performance requirements for aircraft cryotanks. The design allowable stress is assumed to be 34 ksi (234 MPa) [3]. The tank must be able to survive 60,000 thermomechanical cycles (i.e., estimated number of refueling cycles per flight for average aircraft) with a life reduction factor of four [3] yielding a 240,000 cycle criterion. This stress level and cycle count are used to evaluate the candidacy of the tested material for further development as cryotank material.

The S-N curves for wrought and flow-formed Al 6061 are shown in Figure 8. The S-N curve for the flow-formed Al 6061 (blue) compared to wrought material (black) taken from literature [17]. The S-N curves for flow-formed and wrought Al-Li 2195 are shown in Figure 9. The Basquin equation ($S = BN^{-m}$), where S is stress; N is the number of cycles; and B and m are fitting constants, was used for determining the line of best fit. The data for wrought Al 6061 was taken from Yahr [17]. The data was corrected via mean stress conversion with the linear Goodman equation and fatigue life curve fit from Yahr [17]. The flow-formed Al 6061 just meets the cryotank candidacy metrics of surviving 240,000 cycles at 34 ksi (234 MPa). For Al-Li 2195, both the wrought and flow-formed material exceed the candidacy metrics. Flow-formed and wrought Al-Li 2195 are predicted to survive stresses up to ~40 ksi (276 MPa) and 43 ksi (297 MPa) for 240,000 cycles, respectively. The flow-formed and wrought Al-Li 2195 data sets were found to be statistically equivalent by a two-sample t-test at a 5% significance level (α=0.05).

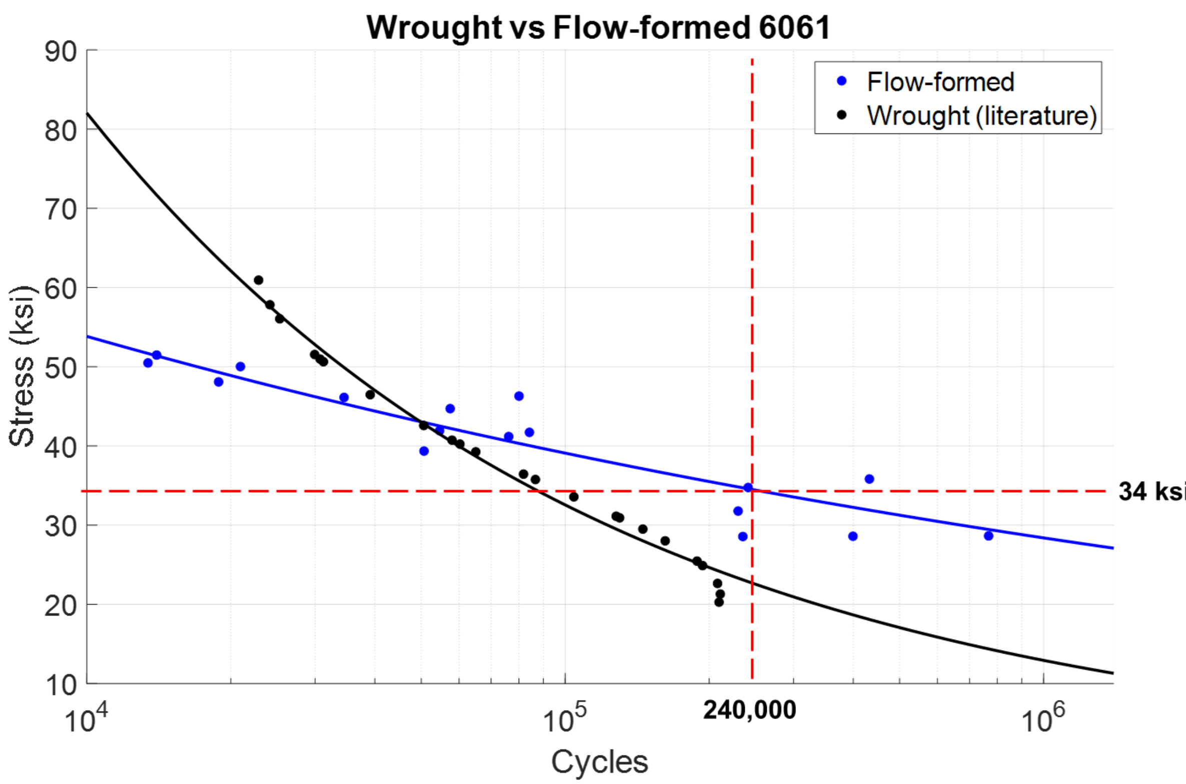

Figure 8. The S-N curve for the flow-formed Al 6061 (blue) compared to wrought material (black) taken from literature [17].

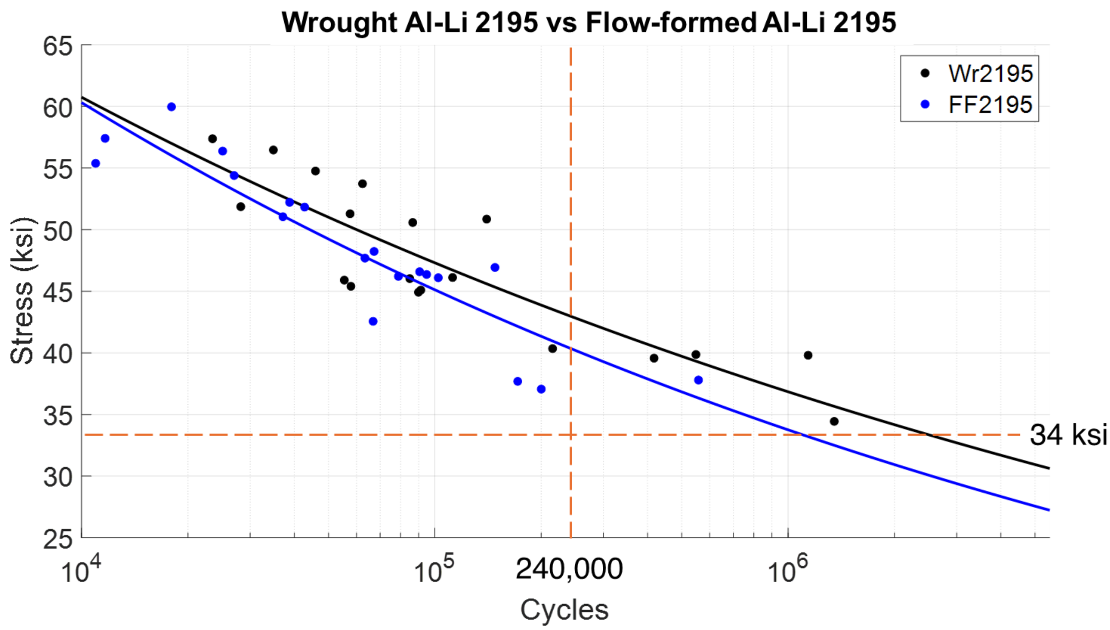

Figure 9. The S-N curves for the flow-formed (blue) and wrought (black) Al-Li 2195.

The S-N curves for flow-formed Al-Li 2195 tested at room and cryogenic temperatures (-321 ºF; -196ºC) are shown in Figure 10. The cryogenic S-N curve highlights the ability of Al-Li 2195 to survive ten times the required number of cycles at the target stress of 34 ksi (234 MPa). At 240,000 cycles, Al-Li 2195 improves from withstanding ~43 ksi (~297 MPa) at room temperature to 59 ksi (407 MPa) at cryogenic temperatures. The mechanical properties of Al-Li 2195 previously have been shown to increase at cryogenic temperatures [18,19], thus it not surprising that the fatigue life also shows improvement. The room temperature and cryogenic S-N curves were shown to be statistically different via a two-sample t-test. The durability of flow-formed Al-Li 2195 to withstand the thermomechanical cycles required for an aircraft appears to be favorable.

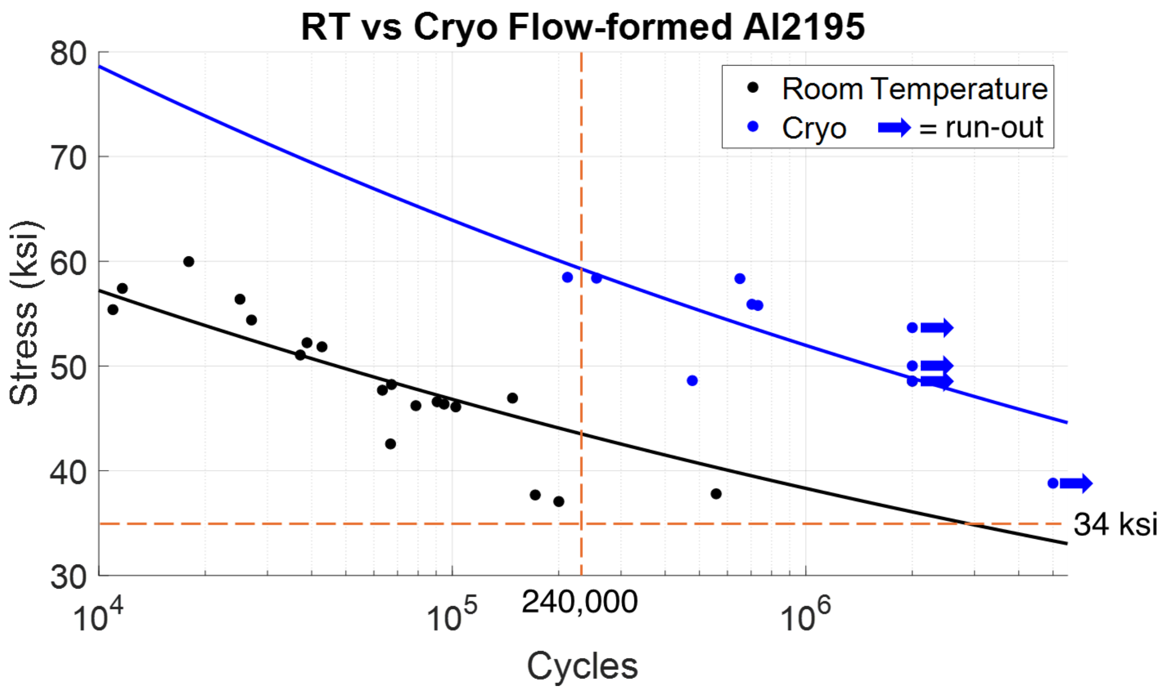

Figure 10. The S-N curves for the flow-formed Al-Li 2195 tested at room temperature (black) and at cryogenic temperature (-321ºF; -196ºC; blue).

Samples with different orientations with respect to rolling or flow-forming processing methods were tested (see Table 1). There were no statistically significant differences found between the different orientations sampled in terms of fatigue life performance. Al 6061 usually has a weak texture, thus lack of influence of directionality (anisotropy) on the fatigue performance is expected. On the other hand, Al-Li 2195 tends to have a stronger texture effect, especially in extruded materials [20], which has been shown to influence fatigue life [21]. Since the processing direction and crystallographic texture can be correlated, the lack of influence of texture on fatigue life performance is notable.

3.3 Fractography

Fracture surfaces from select fatigue test specimens from the flow-formed Al 6061, flow-formed Al-Li 2195 and wrought Al-Li 2195 material were investigated with optical fractography. Optical fractography images (left) and profilometry images (right) are shown for representative samples of flow-formed Al 6061 (a), flow-formed Al-Li 2195 (b), wrought Al-Li 2195 (c) and flow-formed Al-Li Al 2195 tested at cryogenic temperatures (d) in Figure 11.

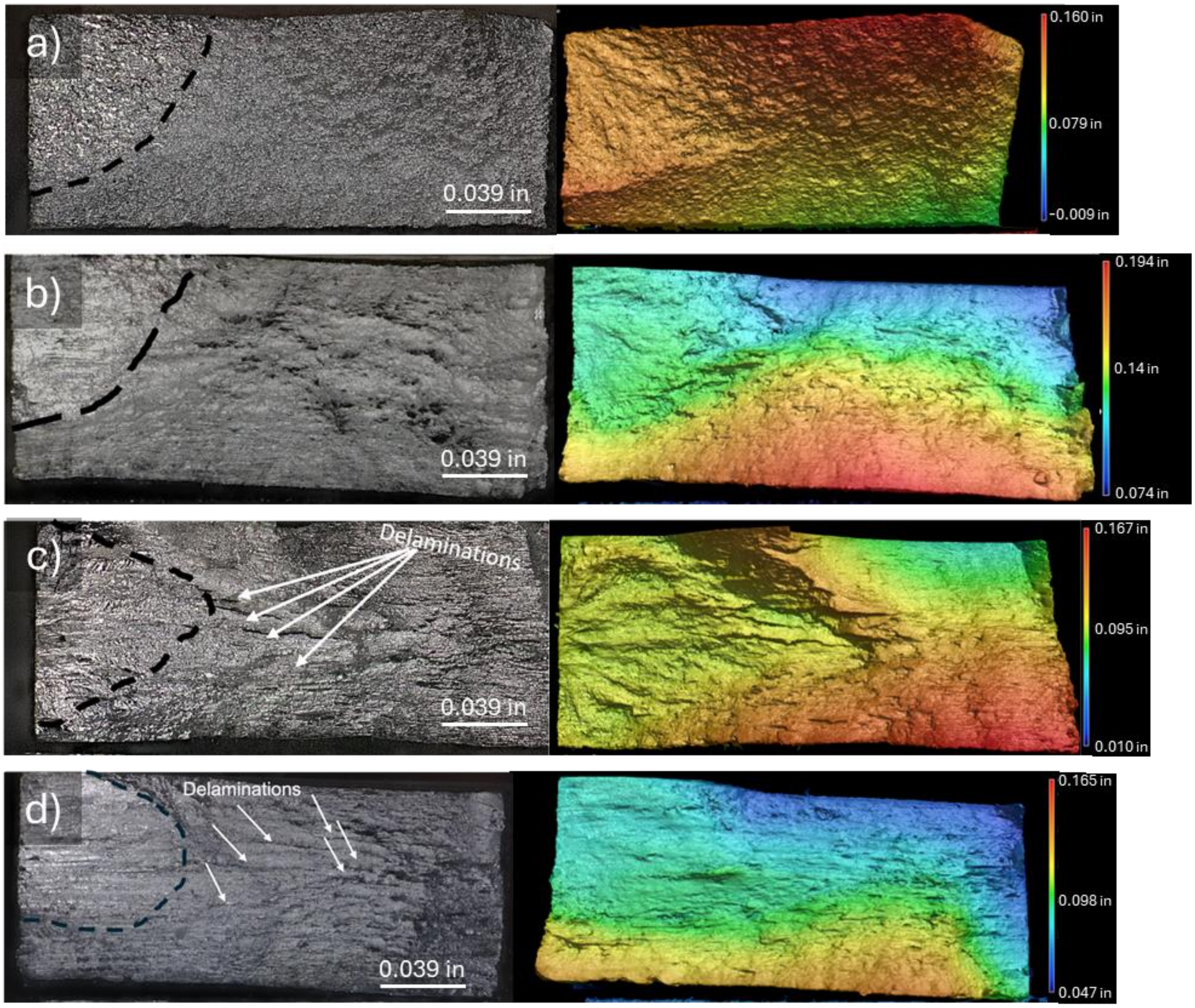

Figure 11. Representative fatigue test specimen fracture surfaces from flow-formed a) Al 6061, b) flow-formed Al-Li 2195, c) wrought Al-Li 2195 and d) flow-formed Al-Li Al 2195 tested at cryogenic temperatures. (Left) Optical image and (right) profilometry image both generated from Keyence microscope. Dashed black line denotes the fatigue crack front.

In the flow-formed Al 6061 and Al-Li 2195 material, most of the fatigue specimen cracks initiated at the corners of the rectangular specimen geometry and propagated to the boundary denoted by the dashed black line on the left-hand optical images (Figure 11a and b). The specimen geometry and surface finish were the driving forces for initiation of the fatigue cracks. There did not appear to be any indication of the flow forming process resulting in material defects that influenced nucleation.

Examination of the surfaces in greater detail using SEM depict radial fatigue cracks progressing from either the edge or corners of the specimen across the specimen for a short distance until they failed via overload fracture. The distance of fatigue crack propagation and corresponding fatigue life is heavily influenced by the stress amplitude. Higher stress amplitude resulted in shorter life and shorter fatigue crack propagation, as expected. The fatigue crack initiates at the corner of the specimen. The fatigue crack region is consistent with fatigue fracture surfaces from other aluminum alloys. The overload regions were characterized as single slant fractures. The overload regions exhibited dimpled rupture, indicating ductile failure via microvoid coalescence (MVC). In flow-formed Al-Li 2195 (Figure 11b), the grain structure was elongated in the long-transverse (LT) dimension of the cross-section, hence some shallow, subtle ridges were observed in the overload region, which correlate with grain boundaries in the material. The sides of the test specimens exhibit some necking in (reduction in cross-sectional area), further indicating a ductile overload failure mode post-fatigue fracture.

Wrought Al-Li 2195 fatigue test specimen fracture surfaces (Figure 11c) demonstrated a similar proclivity for fatigue crack initiation at the corners and edges of the specimen. The fatigue cracks were typically longer and less symmetric that those occurring in the flow formed Al-Li 2195 specimens. The longer fatigue cracks may be indicative of greater cycles to failure assuming similar crack growth rates, and/or increased load carry capacity in the remaining region outside of the fatigue crack. The overload fracture surfaces were a mix of single and double slant fractures. Generally, the fracture features in the overload area were considered ductile with evidence of MVC and some out-of-plane brittle intergranular failures (known as delaminations), which are common in Al-Li alloys, of varying widths and depths.

Within the overload regions, a majority of the specimens exhibited some minor to significant evidence of delamination fracture along the elongated plate grain boundaries in LT direction. Several delaminations are indicated with arrows in top half of the fracture surface in (Figure 11c). The occurrence of delamination was a noticeable difference compared to the flow formed material, which did not exhibit delamination fracture, except when tested at cryogenic temperatures (Figure 11d). In specimens with large delamination cracks in the overload region, the fatigue life measured in number of cycles to failure was generally lower than those without delaminations.

The decreased occurrence of delamination in flowed-formed Al-Li 2195 suggests the microstructure is more resistant to grain boundary cracking than wrought. Flow-formed Al-Li 2195 tested at cryogenic temperatures did show signs of delamination, however delamination cracking is known to be more numerous at cryogenic temperatures [22,23]. This may be associated with a slightly smaller plastic zone size due to the elevated yield strength at cryogenic temperatures, leading to greater plane strain constraint and elevated stress triaxiality which are favorable for delamination.

Prior studies have indicated that delaminations may increase fatigue life [24], which may seem counterintuitive. However, the delamination cracks are energy absorbers and decrease the fatigue crack driving force. The presence of an interior delamination crack causes a transition from plane strain (maximum constraint and stress triaxiality) to plane stress [23]. Longer fatigue life is expected for plane stress conditions, and shorter life for plane strain. Indeed, the fatigue performance of the wrought Al-Li 2195, based on number of cycles to failure, was slightly higher than the flow formed Al-Li 2195, which may partly be attributed to the impact of delamination cracking. Thus, while delamination benefits fatigue performance based on laboratory testing, the presence of the delamination cracks could negatively impact durability when subjected to complex 3D stress states akin to in-service loads.

In light of the delamination behavior, one must question if the test data represent a conservative estimate of performance in service based on linear elastic fracture mechanics principles, where loading may be substantially different from laboratory test conditions. Even if the design is conservative, the delaminations are secondary cracks that propagate on grain boundaries (normal to the Short-Transverse (S-T) plane). Al-Li alloys are known for poor S-T toughness [25–27].

Thus, under the right stress state, there is potential for delamination cracks to preferentially grow at an accelerated rate under complex loading conditions not replicated via testing. Flow-formed material, less prone to delamination cracking, could show higher durability than wrought material in complex loading scenarios, though further testing is required to confirm the hypothesis.

The reason why the flow formed Al-Li 2195 microstructure exhibits less delamination cracking will require further examination to explain, which is outside of the scope of this work. However, some rationale may be proposed based on inference using existing knowledge.

Delamination cracking is associated with several synergistic factors:

1. Long, flat (lamellar) grain boundaries [16,25,27],
2. Unfavorable, unrecrystallized preferred grain orientations (texture) paired together that result in a lack of slip transfer at the grain boundary [28,29],
3. High aspect ratio T1 precipitates in the grain boundary plane (microcrack nucleation sites) that may separate from the matrix on one side [28],
4. High dislocation density due to planar slip bands intersecting the grain boundary as a result of shearing matrix delta prime (δ') precipitates [28–33].

The flow-formed microstructure may impact some of these factors due to the flow forming process. First, long, flat grain boundaries may be retained. However, these boundaries may become less planar as a result of material flow patterns, a feature documented previously in [10]. Additionally, the high level of deformation may introduce more substructure. These two grain morphology changes may slightly improve delamination resistance by making the crack path more tortuous, increasing the difficulty for the crack to extend long distances. This may be most noticeable in the stiffener regions where the grain morphology is highly curved due to material flow [10]. However, there was insufficient material within the stiffeners to produce standard fatigue test specimens in this study.

To compare the role of texture in flow-formed and wrought Al-Li 2195, a representative cross-section from the radial-axial plane for one of the FF Al-Li 2195 cylinder wall sections was mapped using electron backscattered diffraction (EBSD) and is presented in Figure 12. Recrystallization was observed closer to the outer mold line surface (surface directly in contact with rollers) with larger grain sizes present likely occurring during heat treatment. These grains retained the general elongated morphology typical of wrought plate, but with reduced aspect ratio (increased grain thickness and reduced length). Further away from the outer mold line (OML) surface, some bands of highly deformed, unrecrystallized, refined grains are present. Some waviness of the grain boundaries has been observed with optical microscopy, particularly in an orthogonal plane like the radial-circumferential plane.

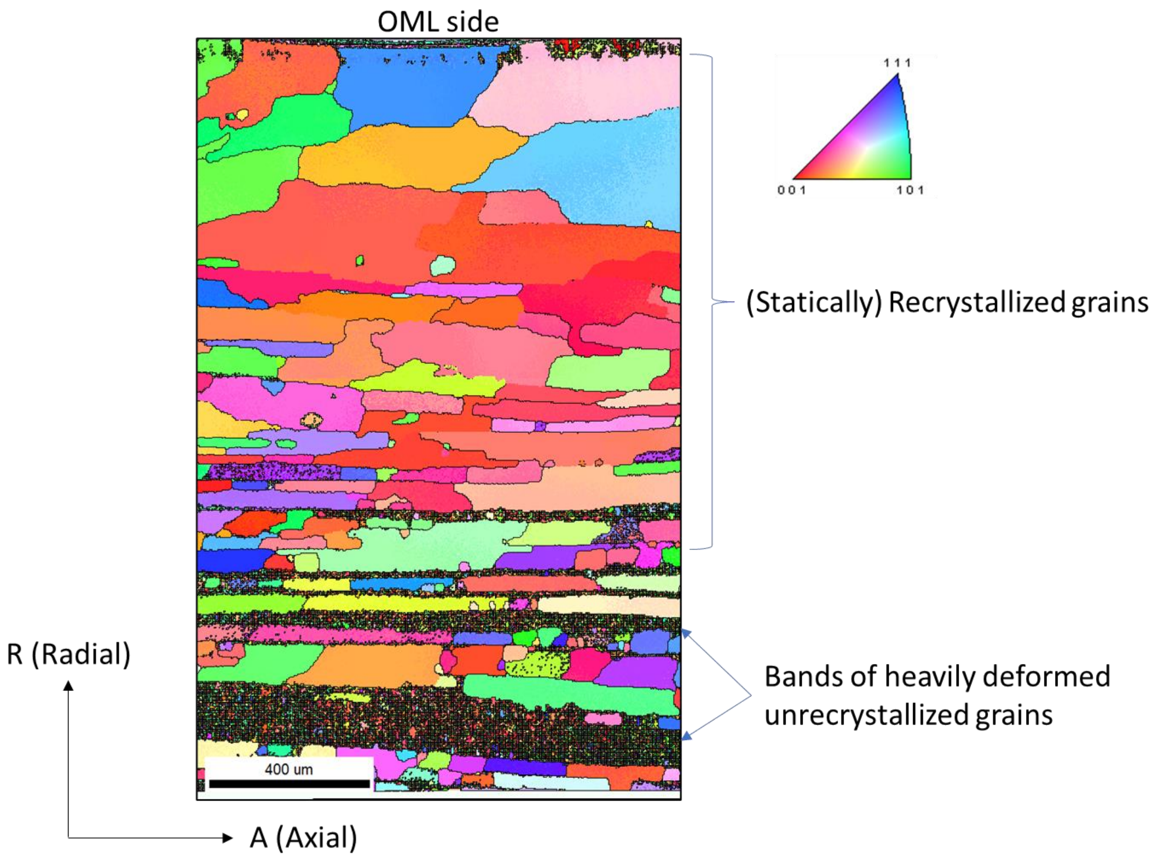

Figure 12. EBSD inverse pole figure map indicating recrystallization within the wall of the Al-Li 2195 flow-formed cylinder.

The flow forming process may modify the texture of the material. Wrought Al-Li plate is most commonly produced via rolling [27]. Rolling often produces a strong texture [29,34,35]. Flow forming may reduce the strength of this texture, and/or produce a preferred texture different from that of conventional wrought products (rolled plate). Texture analysis was performed on the sample referenced above to explore this hypothesis. Pole figures were plotted from the EBSD data in Figure 12 and are presented in Figure 13a. To contrast this texture, EBSD pole figures from Al-Li wrought plate displaying a typical rolled texture are presented in Figure 13. EBSD pole figures from a) Al-Li 2195 flow-formed wall section (RD = axial direction and TD = radial direction of the flow-formed cylinder) and b) rolled Al-Li 2195 plate. The observed flow-formed texture has similar strength to the wrought plate, measured statistically in the form on multiples of a random distribution (4.6 vs. 5.2, respectively). However, the texture has evolved due to recrystallization. The pole figure plots revealed cube or ND-rotated cube texture components that are characteristic of static recrystallization processes for face-centered cubic metals. Whereas the typical rolling texture is comprised of rolling texture components, particularly the brass orientation. The recrystallization most likely occurred during solution heat treatment (SHT) to the -T6 temper. A weakening of the typical wrought texture and development of a recrystallization texture may, at least partially, explain the reduction in observed delaminations for flow-formed Al-Li 2195 versus wrought.

The early generations of Al-Li alloys were known to have significant concerns over planar slip, strong texture (anisotropy), and weak S-T plane (normal to the longitudinal – long-transverse (L-LT) grain boundary plane) properties [24]. In prior work by Rao and Ritchie [24], they noted that newer generation alloys were processed to reduce texture and anisotropy through the incorporation of a (partial) recrystallization annealing treatment [27], which resulted in reduced fatigue performance. Thus, the increased fraction of recrystallization texture components in the flow formed material may have improved delamination resistance but slightly reduced fatigue performance. Prior work suggests that introducing an anneal prior to SHT (known as a recrystallization anneal), may better control the extent of recrystallization that occurs during SHT. This additional thermal processing step may be utilized if less recrystallization is desired [27]; however, further exploration of the impact of delaminations under complex loading on durability is needed.

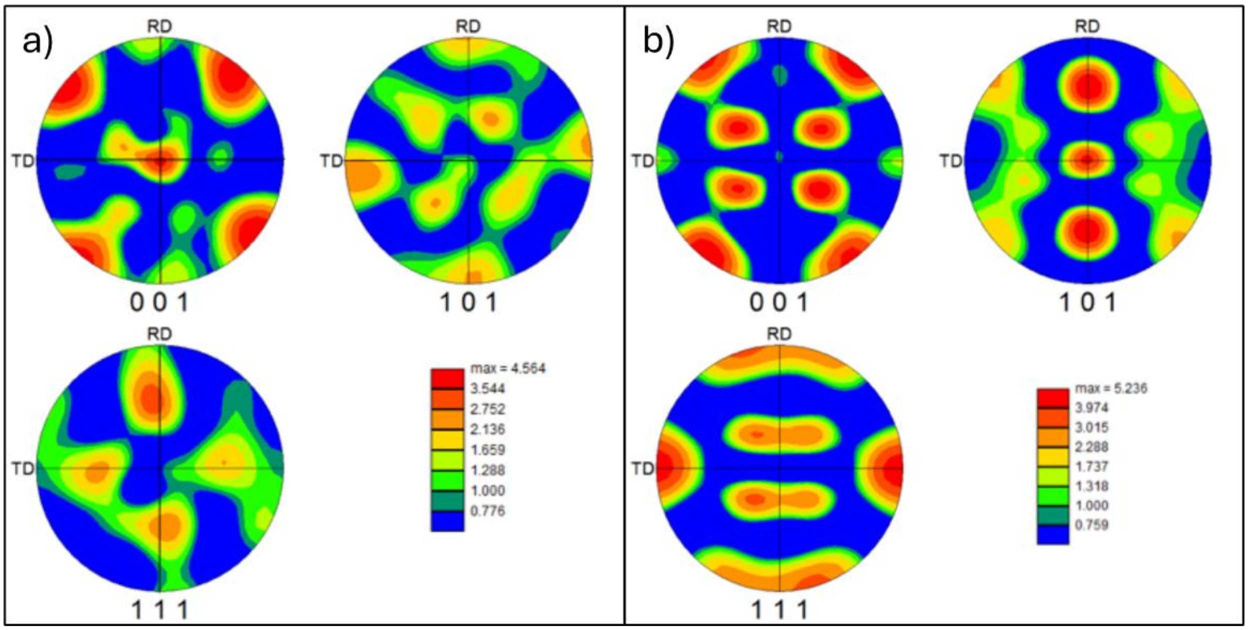

Figure 13. EBSD pole figures from a) Al-Li 2195 flow-formed wall section (RD = axial direction and TD = radial direction of the flow-formed cylinder) and b) rolled Al-Li 2195 plate.

4.0 Conclusion

Flow-formed aluminum alloys were evaluated for use as cryotank material in aircraft by measuring residual stresses and fatigue life performance. The failed fatigue specimen fracture surfaces were analyzed to understand the role of flow-forming on the failure mechanism. The main take-aways from the work are:

- Flow-formed Al-Li 2195 did not show significant residual stresses
- Flow-formed Al-Li 2195 demonstrated near-equivalent fatigue life to wrought Al-Li 2195 and showed decreased levels of delamination that could result in increased service life
- Flow-formed Al-Li 2195 and Al 6061 met or exceeded estimated fatigue life requirements for aviation cryotanks at room temperature
- Flow-formed Al-Li 2195 exceeded fatigue life requirements at cryotemperatures

- No discernable orientation dependence for wrought or flow formed Al-Li 2195 and Al 6061 fatigue life was observed
- Fractography revealed reduced delamination in flow formed versus wrought Al-Li 2195 specimens attributed to grain morphological and texture changes due to flow forming

The S-N curves for flow-formed materials, specifically Al-Li 2195 and Al 6061, provided novel evidence of the durability of such materials. Further testing is warranted to understand the performance of materials under more realistic flight conditions, not simply uniaxial tension. The high-rate efficiencies of the spin forming process coupled with the demonstrated durability are an attractive combination for further design and development of flow-formed metallic cryotanks.

5.0 References

[1] Boddorff, A. K., “Choosing the Right Stuff: Material Selection for Liquid Hydrogen Aircraft Cryotanks,” NASA/TM-20250007133, July 2025.

[2] Verstraete, D., Hendrick, P., Pilidis, P., and Ramsden, K., “Hydrogen Fuel Tanks for Subsonic Transport Aircraft,” International Journal of Hydrogen Energy, Vol. 35, No. 20, 2010, pp. 11085–11098. https://doi.org/10.1016/j.ijhydene.2010.06.060

[3] Brewer, G. D., “Hydrogen Aircraft Technology,” Routledge, New York, 2017. https://doi.org/10.1201/9780203751480

[4] Bagarello, S., Campagna, D., and Benedetti, I., “A Survey on Hydrogen Tanks for Sustainable Aviation,” Green Energy and Intelligent Transportation, Vol. 4, No. 4, 2025, p. 100224. https://doi.org/10.1016/j.geits.2024.100224

[5] Aceves, S. M., Espinosa-Loza, F., Ledesma-Orozco, E., Ross, T. O., Weisberg, A. H., Brunner, T. C., and Kircher, O., “High-Density Automotive Hydrogen Storage with Cryogenic Capable Pressure Vessels,” International Journal of Hydrogen Energy, Vol. 35, No. 3, 2010, pp. 1219–1226. https://doi.org/10.1016/j.ijhydene.2009.11.069

[6] Satyapal, S., Petrovic, J., Read, C., Thomas, G., and Ordaz, G., “The U.S. Department of Energy’s National Hydrogen Storage Project: Progress towards Meeting Hydrogen-Powered Vehicle Requirements,” Catalysis Today, Vol. 120, Nos. 3–4, 2007, pp. 246–256. https://doi.org/10.1016/j.cattod.2006.09.022

[7] Stoner, M. C., Hehir, A. R., Ivanco, M. L., and Domack, M. S., “Cost-Benefit Analysis for the Advanced Near Net Shape Technology (ANNST) Method for Fabricating Stiffened Cylinders,” NASA/TM-2016-219192, May 2016.

[8] Frederic, P., “Advanced Metallic Fuselage Cost Study,” NASA/CR-20240011427, September 2024.

[9] Tayon, W. A., Rudd, M. T., Domack, M. S., and Hilburger, M. W., “Development of Advanced Manufacturing Approaches for Single-Piece Launch Vehicle Structures,” NASA/TM–20210026743, January 2022.

[10] Tayon, W. A., Domack, M. S., and Wagner, J. A., “Characterization of 10-Ft. Diameter, Aluminum Alloy 2219 Integrally Stiffened Cylinders,” NASA/TM-2019-220260, 2019.

[11] Tayon, W., Domack, M., Wagner, J., Taminger, K., Hoffman, E., and Newman, S., “Development and Characterization of the Integrally Stiffened Cylinder (ISC) Process for Launch Vehicles and Aircraft Fuselage Structures,” Light Alloys 2021, 2021. https://doi.org/10.1007/978-3-030-65396-5_46

[12] Domack, M., Wagner, J., and Tayon, W., “Integrally Stiffener Cylinder (ISC) Process Development,” Strategic Interchange Meeting, Ahlen, Germany, Jan 30, 2015.

[13] Prime, M. B., and DeWald, A. T., “The Contour Method,” Practical Residual Stress Measurement Methods, John Wiley & Sons, Ltd, 2013, pp. 109–138. https://doi.org/10.1002/9781118402832.ch5

[14] Pagliaro, P., Zuccarello, B., Prime, M. B., Clausen, B., Lovato, M. L., Steinzig, M. L., Swenson, H., Robinson, J. S., and Schajer, G. S., “S113 Mapping Multiple Residual Stress Components Using the Contour Method and Superposition,” Powder Diffraction, Vol. 23, No. 2, 2008, pp. 187–187. https://doi.org/10.1154/1.2951812

[15] Roy, M. J., Stoyanov, N., Moat, R. J., and Withers, P. J., “pyCM: An Open-Source Computational Framework for Residual Stress Analysis Employing the Contour Method,” SoftwareX, Vol. 11, 2020, p. 100458. https://doi.org/10.1016/j.softx.2020.100458

[16] Prasad Prasad, N., Gokhale, A., and Wanhill, R. J. H., "Aluminum-Lithium Alloys: Processing, Properties, and Applications," Butterworth-Heinemann, 2013.
[17] Yahr, G. T., "Fatigue Design Curves for 6061-T6 Aluminum," Journal of Pressure Vessel Technology, Vol. 119, No. 2, 1997, pp. 211–215. https://doi.org/10.1115/1.2842286
[18] Nayan, N., Narayana Murty, S. V. S., Jha, A. K., Pant, B., Sharma, S. C., George, K. M., and Sastry, G. V. S., "Mechanical Properties of Aluminium–Copper–Lithium Alloy AA2195 at Cryogenic Temperatures," Materials & Design, Vol. 58, 2014, pp. 445–450. https://doi.org/10.1016/j.matdes.2014.02.024
[19] Cai, Q., Chang, Z., Zhang, W., Cao, G., Li, H., Jiang, B., Zhang, Z., and Zhang, H., "Investigation on the Mechanical Properties and Microstructural Evolution of Friction Stir Welded 2195 Aluminum Alloy at Cryogenic Temperature," Materials Characterization, Vol. 225, 2025, p. 115152. https://doi.org/10.1016/j.matchar.2025.115152
[20] Hales, S. J., and Hafley, R. A., "Texture and Anisotropy in Al-Li Alloy 2195 Plate and near-Net-Shape Extrusions," Materials Science and Engineering: A, Vol. 257, No. 1, 1998, pp. 153–164. https://doi.org/10.1016/S0921-5093(98)00834-X
[21] Strohmann, T., Breitbarth, E., Besel, M., Zaunschirm, S., Witulski, T., and Requena, G., "Damage Mechanisms and Anisotropy of an AA7010-T7452 Open-Die Forged Alloy: Fatigue Crack Propagation," Materials, Vol. 15, No. 11, 2022, p. 3771. https://doi.org/10.3390/ma15113771
[22] Venkateswara Rao, K. T., Yu, W., and Ritchie, R., "Cryogenic Toughness of Commercial Aluminum-Lithium Alloys: Role of Delamination Toughening," Metallurgical and Materials Transactions A, Vol. 20A, 1989, pp. 485–497.
[23] Kalyanam, S., Beaudoin, A. J., Dodds, R. H., and Barlat, F., "Delamination Cracking in Advanced Aluminum–Lithium Alloys – Experimental and Computational Studies," Engineering Fracture Mechanics, Vol. 76, No. 14, 2009, pp. 2174–2191. https://doi.org/10.1016/j.engfracmech.2009.06.010
[24] Venkateswara Rao, K. T., and Ritchie, R. O., "Fatigue of Aluminium--Lithium Alloys," International Materials Reviews, Vol. 37, 1992, pp. 153–186.
[25] Venkateswara Rao, K. T., and Ritchie, R. O., "Mechanisms Influencing the Cryogenic Fracture-Toughness Behavior of Aluminum-Lithium Alloys," Acta Metallurgica et Materialia, Vol. 38, No. 11, 1990, pp. 2309–2326.
[26] Rioja, R. J., "Fabrication Methods to Manufacture Isotropic Al-Li Alloys and Products for Space and Aerospace Applications," Materials Science and Engineering: A, Vol. 257, No. 1, 1998, pp. 100–107. https://doi.org/10.1016/s0921-5093(98)00827-2
[27] Rioja, R. J., and Liu, J., "The Evolution of Al-Li Base Products for Aerospace and Space Applications," Metallurgical and Materials Transactions A, Vol. 43, No. 9, 2012, pp. 3325–3337. https://doi.org/10.1007/s11661-012-1155-z
[28] Tayon, W., Crooks, R., Domack, M., Wagner, J., Beaudoin, A., and McDonald, R., "Mechanistic Study of Delamination Fracture in Al-Li Alloy C458 (2099)," presented at the 12th International Conference on Fracture (ICF12), Ottawa, Canada, 2009.
[29] Tayon, W., Crooks, R., Domack, M., Wagner, J., and Elmustafa, A. A., "EBSD Study of Delamination Fracture in Al–Li Alloy 2090," Experimental Mechanics, Vol. 50, No. 1, 2010, pp. 135–143. https://doi.org/10.1007/s11340-008-9202-9
[30] Blankenship Jr, C. P., Hornbogen, E., and Starke Jr, E. A., "Predicting Slip Behavior in Alloys Containing Shearable and Strong Particles," Materials Science and Engineering: A, Vol. 169, Nos. 1–2, 1993, pp. 33–41. http://dx.doi.org/10.1016/0921-5093(93)90596-7

[31] Csontos, A., "Microstructural Effects on the Slip and Fracture Behavior of Isotropic Al-Li-Cu-X Alloys," University of Virginia, 2001.
[32] Csontos, A., and Starke, E., "The Effect of Processing and Microstructure Development on the Slip and Fracture Behavior of the 2.1 Wt Pct Li AF/C-489 and 1.8 Wt Pct Li AF/C-458 Al-Li-Cu-X Alloys," Metallurgical and Materials Transactions A, Vol. 31, No. 8, 2000, pp. 1965–1976.
[33] Csontos, A. A., and Starke, E. A., "The Effect of Inhomogeneous Plastic Deformation on the Ductility and Fracture Behavior of Age Hardenable Aluminum Alloys," International Journal of Plasticity, Vol. 21, No. 6, 2005, pp. 1097–1118. https://doi.org/10.1007/s11661-000-0224-x
[34] Contrepois, Q., Maurice, C., and Driver, J. H., "Hot Rolling Textures of Al-Cu-Li and Al-Zn-Mg-Cu Aeronautical Alloys: Experiments and Simulations to High Strains," Materials Science and Engineering: A, Vol. 527, Nos. 27–28, 2010, pp. 7305–7312. https://doi.org/10.1016/j.msea.2010.07.095
[35] Bate, P. S., Huang, Y., and Humphreys, F. J., "Development of the 'Brass' Texture Component during the Hot Deformation of Al–6Cu–0.4Zr," Acta Materialia, Vol. 52, No. 14, 2004, pp. 4281–4289. https://doi.org/10.1016/j.actamat.2004.05.044

Appendix A. Full Organizational Model

Table 2 lists the specific results from the fatigue life tests performed that were used to create the S-N curves.

Table 2. Results from fatigue life testing from all specimens tested.

Alloy	Temperature	Orientation/Location	Stress (ksi)	Cycles
Wrought Al-Li 2195	Room Temperature	Rolling	53.7	6.2E+04
			44.9	9.0E+04
			50.9	1.4E+05
			39.8	1.1E+06
			39.9	5.5E+05
			51.3	5.8E+04
			46.0	8.5E+04
			51.9	2.8E+04
			46.1	1.1E+05
			54.8	4.6E+04
		45	50.6	8.7E+04
			39.6	4.2E+05
			56.5	3.5E+04
			45.1	9.1E+04
			45.4	5.8E+04
			34.4	1.4E+06
			45.9	5.5E+04
			57.4	2.3E+04
			40.3	2.2E+05
Flow-Formed Al-Li 2195	Cryogenic	Between Stiffeners	55.8	7.3E+05
			58.5	2.1E+05
			58.3	6.5E+05
			58.4	2.6E+05
			48.6	4.8E+05
			55.9	7.0E+05
			53.7	2.0E+06*
			38.8	5.0E+06*
			50.0	2.0E+06*
			48.6	2.0E+06*
	Room Temperature		37.8	5.6E+05
			52.2	3.9E+04
			56.4	2.5E+04
			51.8	4.3E+04
			57.4	1.2E+04

			47.7	6.3E+04
			60.0	1.8E+04
			48.2	6.7E+04
			37.1	2.0E+05
			42.6	6.7E+04
			54.4	2.7E+04
			37.7	1.7E+05
			55.4	1.1E+04
			51.1	3.7E+04
		Behind Stiffener	46.9	1.5E+05
			46.6	9.1E+04
			46.1	1.0E+05
			46.2	7.9E+04
			46.4	9.5E+04
Flow-formed Al 6061	Room Temperature	Axial	31.8	2.3E+05
			50.5	1.3E+04
			50.0	2.1E+04
			29.4	1.8E+06
			44.7	5.7E+04
			46.3	8.0E+04
			35.8	4.3E+05
			51.5	1.4E+04
			41.2	7.6E+04
			41.7	8.4E+04
		Circumferential	46.1	3.4E+04
			28.6	2.4E+05
			28.6	4.0E+05
			41.9	5.5E+04
			34.7	2.4E+05
			48.1	1.9E+04
			28.6	7.7E+05
			39.3	5.1E+04

*Test stopped due to hitting run-out limit.